To appear in the Astrophysical Journal

Fourier-Resolved Spectroscopy of AGN using XMM-Newton data: I. The 3-10 keV band results

I.E. Papadakis[1,2], Z. Ioannou[2,1], D.Kazanas[3]

ABSTRACT

We present the results from the Fourier Resolved Spectroscopy of archival *XMM-Newton* data of five AGN, namely, Mrk 766, NGC 3516, NGC 3783, NGC 4051 and Ark 564. This work supplements the earlier study of MCG-6-30-15 as well as those of several Galactic Black Hole Candidate sources. Our results exhibit much larger diversity than those of Galactic sources, a fact we attribute to the diversity of their masses. When we take into account this effect and combine our results with those from Cyg X-1, it seems reasonable to conclude that, at high frequencies, the slope of the Fourier-resolved spectra in accreting black hole systems decreases with increasing frequency as $\propto f^{-0.25}$, irrespective of whether the system is in its High or Low state. This result implies that the flux variations in AGN are accompanied by complex spectral slope variations as well. We also find that the Fe Kα line in Mrk 766, NGC 3783 and NGC 4051 is variable on time scales ~ 1 day $-$ 1 hour. The iron fluorescence line is absent in the spectra of the highest frequencies, and there is an indication that, just like in Cyg X-1, the equivalent width of the line in the Fourier-resolved of AGN decreases with increasing frequency.

Subject headings: Galaxies: Active, Galaxies: Seyfert, X–Rays: Galaxies

1. Introduction

Our generic notion of the central engine of Active Galactic Nuclei (AGN) and, in general, also that of compact Galactic sources such as neutron stars and black holes powered by

[1]Physics Department, University of Crete, Heraklion, 71003, Crete, Greece

[2]IESL, Foundation for Research and Technology-Hellas, 711 10 Heraklion,Crete, Greece

[3]Laboratory for High Energy Astrophysics, NASA, Goddard Space Flight Center, Code 661, Greenbelt, MD 20771, USA

accretion, involves a geometrically thin, optically thick accretion disk that emits locally as a black body "sandwiched" between a hot ($\sim 10^9$ K) corona which up-Comptonizes the disk thermal radiation to produce the ubiquitous X–ray emission associated with this class of objects. Despite the compelling theoretical arguments in support of this picture, independent supporting evidence of the specific geometrical arrangement is hard to come by. For one, only a small fraction of the very broad band multicolor black body spectrum of the putative disk is covered by our instruments making hard the detailed assessment of the form of its spectrum. Second, the Comptonization spectrum of the hot corona provides information for only the integral of the Comptonization parameter along our line of sight, rather than the conditions of the local plasma.

Independent support of the above generic picture has been sought in distinct spectral and timing signatures implied by the specific geometric arrangement. More specifically, the Fe Kα fluorescence line at $E = 6.4$ keV as well as the so-called reflection 'hump', the product of reprocessing the X–rays of the hot corona by the matter of the underlying accretion disk, are thought to provide a direct measure of the above geometry. Furthermore, the Keplerian motion of the reprocessing matter in the disk would lead to a rather broad profile for this spectral feature. Indeed, the detection of such a feature in the ASCA spectra of many Seyfert galaxies (*e.g.* Nandra et al. 1997) seems to provide a confirmation of these notions. At the same time it has been argued that detailed X–ray spectroscopy of the iron line emission features can provide information on the location and kinematics of the cold material within a few gravitational radii of the event horizon.

In addition to the above features, a measure of the size of the X–ray emitting region, independent of its spectral properties, can be obtained from time variability studies. In the specific case of emission produced by the Comptonization process, Kazanas, Hua & Titarchuk (1997) argued that timing observations are the only way to estimate the density of the emitting plasma (in contrast to its column density provided by the Comptonization spectra) and thus peek into the dynamics of the accretion flow. The principal method of characterizing the variability of accretion powered sources has been the measurement of the Power Spectral Density function (PSD) of their X–ray light curves, which in the case of AGN, were shown to be simple power laws with occasional "breaks" in the slope at sufficiently low frequencies. However, unlike the Comptonization spectra whose slopes and cut-offs can be related directly to the physical parameters of the emitting plasma, there is no simple model that relates in a direct fashion the shape of the PSD to the physics of the accretion flow.

Recently, a novel approach in the study of accretion powered sources, which combines variability and spectral information, has been taken by Revnivtsev, Gilfanov & Churazov (1999). Using *RXTE* data, they measured the power spectrum, and hence the amplitudes of the Fourier components, of Cygnus X-1 in its hard state for different energies. Then, at each energy band, they assembled the Fourier amplitudes within a given Fourier frequency range, say Δf, to produce the so-called Fourier-Resolved (FR) spectrum of the band Δf. The process was repeated to obtain the FR spectra of many such frequency bands, thereby combining the information provided by the time variability with the simplicity of the insights provided by the "energy spectra". Their main conclusions were that: (a) the soft component of the spectra (thought to represent thermal emission from the innermost parts of the accretion disk) is absent from the Fourier resolved spectra, indicating that it is not variable on time scales less than ~ 100 s, (b) The FR spectra (in the frequencies that are determined) are power-laws which become progressively harder with increasing Fourier frequency, and (c) the Fe Kα line and reflection components become less pronounced as the Fourier frequency increases.

Using the same approach, the X–ray continuum spectral variability of the Galactic black hole binaries (GBHs) GX 339-4 and 4U 1543-47, during its 2002 outburst, as well as Cyg X-1 in its soft state have also been studied respectively by Revnivtsev, Gilfanov & Churazov (2001); Reig et al.(2006), and Revnivtsev, Gilfanov & Churazov (2000). The Fourier-resolved spectroscopy (FRS) has also been used to study the nature of the quasi-periodic oscillations in neutron stars (Gilfanov, Revnivtsev, & Molkov 2003, Gilfanov & Revnivtsev 2005; Sobolewska & Życki 2006).

Recently, Papadakis, Kazanas, & Akylas (2005) applied for the first time the same technique to an AGN, namely to the *XMM-Newton* observations of MCG -6-30-15. Their results were similar to those of Revnivtsev et al. (1999) in the case of Cyg X-1 in its hard state, with the exception of the soft excess component at energies $E \lesssim 1$ keV which was present in the spectra of all Fourier bands, implying variability of this component in all frequency bands examined, in contrast with the behavior of Cyg X-1.

In the present note we apply the method of Fourier-resolved spectroscopy to five more AGN, using observations by *XMM-Newton*. Our aim is to explore the spectral variability properties of a sizable sample of AGN, as implied by the application of FRS, in order to investigate whether potential common trends and similarities with GBHs. In this work we report our results regarding the AGN spectral variability properties at energies above 3 keV. In this energy band, the AGN time-average spectra are dominated by a power-law continuum. Reflection features like the iron Kα line, and the associated absorption edge, appear as well. At lower energies, many AGN show considerable complexity, caused either by the presence of warm absorbing material and/or by the presence of the so-called soft-excess emission component. In principle, the warm absorber can respond to variations of the underlying continuum while the soft excess emission is often observed to be variable.

Consequently, FRS can be used in order to study in detail their variability properties. We plan to present the results from such a study in the near future.

In §2 and §3 we discuss the data sets and the methodology we use, respectively. In §4 we present the results from various model fits to the time average and FR spectra of the objects in our sample. Finally, in §5 and §6 we discuss our results briefly in the context of theoretical ideas and models presently in the literature and we present our summary and future plans, respectively.

2. Observations & Data Reduction and Analysis Method

XMM-Newton, with the large effective area of its instruments and its capability to observe a source continuously for a period up to $\sim$ 1.3 days, can provide long duration light curves that are appropriate in order to obtain accurate Fourier-resolved spectra for the AGN. To this end, we searched the *XMM-Newton* public data archive for those AGN which have been observed, at least once, for an on-source exposure time larger than 100 ks. Prior to April 2005, there were 5 AGN which satisfied this criterion, namely Mrk 766, NGC 3516, NGC 3783, NGC 4051, and Ark 564. For those objects, we also considered all the available observations in the archive, as in principle we can combine the data from different observations in order to estimate the FR spectra as accurately as possible.

Apart from the criterion regarding the exposure time, we also required that the objects show significant variations in all the energy bands that we consider (see below). For this reason, we used 1000 s binned light curves (in this way the source counts in each bin were, on average, larger than 20) and applied the usual χ^2 test. We found that all sources displayed variations significant at more than the 95% confidence level, in all energy bands, except from the November 2001 observation of NGC 3516. Significant variations can be detected during the April 2001 observation of this source. Although the on-source exposure time in this case is smaller than 100 ks, we decided to keep the source in our sample and use the data from this observation to study its FR spectra. As for the shorter observations of the other sources, none of them showed significant variations, except from the November 2002 observation of NGC 4051. In fact, the time-average spectra of the source during the 2001 and 2002 observations are so different that we decided to study the two FR spectra separately.

In Table 1 we list the details of all the observations that we have used in the present work. All data have been reduced using XMMSAS v6.1.0. We use data from the European Photon Imaging Camera (EPIC) pn detector only. All sources were observed on-axis. With an average count rate of less than $\sim$ 30 cts s^{-1} in all cases, photon pile-up is negligible for the PN detector, as was verified using the XMMSAS task *epatplot*. Source counts were accumulated using a circular region of $40''$ around the position of the source. Background data were extracted from a similar size, source free, region on the chip. We selected single and double pixel events (PATTERN$= 0-4$) in the energy range from 200 eV to 10 keV.

The background was in general low and stable throughout all the observations, with the exception of short periods at the start and/or at the end of each observation. Data from these periods of high background levels were removed. The "exposure times" listed in the third column of Table 1 refer to the total on-source exposure time of the pn detector, after these high background level periods are removed.

In Figures 1 and 2 we show the $0.2-10$ keV, background-subtracted, 100 s binned light curves, extracted from the data of all observations that we consider in this work. All light curves are normalized to the lowest count rate observed. In this way, one can easily judge their "quality". For example, NGC 3516 shows the smallest amplitude variations (min-to-max amplitude ratio of $\sim 1.5-1.6$). Its light curve is also short, and of low signal-to-noise ratio. On the other hand, NGC 4051 shows the largest amplitude variations (with a min-to-max ratio of ~ 15 during the 2001 observation). The longest light curve is that of NGC 3783. This source is bright, and also displays significant variations on all sampled time scales, with a maximum amplitude of ~ 2.5.

3. Analysis Method

In this section we present in some detail the theory on which FRS is based, as this is still a novel analysis method, rarely used in the variability studies of compact objects. The method is based on the fact that any stationary process can be represented as the "sum" of sine and cosine functions (e.g. Priestley 1989). More specifically, let us denote with $X(t)$ a stationary process, i.e. the time variable emitted flux from an AGN, for example. Then, $X(t)$ can be represented as,

$$X(t) = \int_0^{+\infty} \cos(\omega t) dU(\omega) + \int_0^{+\infty} \sin(\omega t) dV(\omega).$$

The integrals above are stochastic and defined in the mean-square sense (Priestley 1989). As for the stochastic processes $dU(\omega)$ and $dV(\omega)$, they are orthogonal (i.e. their increments at different frequencies are uncorrelated) and, more importantly, for each frequency, ω, one can write,

$$\langle |dU(\omega)|^2 \rangle = \langle |dV(\omega)|^2 \rangle = h(\omega) d\omega,$$

where the brackets denote the mean of a random variable, and $h(\omega)$ is the (non-normalized) power spectral density function of the stationary process $X(t)$. In other words, the amplitude of the sine and cosine (random) functions that can be used to represent $X(t)$ are related to the power spectral density function of $X(t)$. This is the 'crucial' property that we can use in practice to estimate the amplitude of the sine and cosine functions (*i.e.* the "Fourier components" of the random process under study).

Suppose we observe the X–ray emission from an AGN N times over a period of T s. Let us denote with Δt the interval of each observation (so that $N\Delta t = T$), and with $x(E, t_i)(i = 1, 2, \ldots, N)$ the N points of the light curve (in units of counts s^{-1}). Note that we have assumed we observe the object at a particular energy band of (median) energy E. Using the discrete Fourier-transform of the light curve, we can estimate the power spectral density function (PSD) of the random process (whose one realization is the light curve at hand) as follows,

$$P(E, f_j) = \frac{2\Delta t}{N} \left| \sum_{i=1}^{N} x(E, t_i) e^{-2\pi f_j t} \right|^2 . \tag{1}$$

The units are (counts s^{-1})^2 Hz^{-1}, and the PSD is estimated at the set of frequencies, $f_j = j/T, j = 1, ..., N/2$. Based on what we mentioned above, the quantity,

$$R(E, f_j) = \sqrt{P(E, f_j)\Delta f} \ \text{(counts s}^{-1}\text{)}, \tag{2}$$

(where $\Delta f = 1/T$) can be considered as an estimate of the amplitude of the Fourier components with frequency f_j.

Suppose now that we have obtained N_E light curves at different energy bands with median energy $E_k, k = 1, 2, \ldots, N_E$. If, for each one, we estimate the amplitude of the Fourier components with frequency f_j, i.e. $R(E_k, f_j)$, then the plot of $R(E_k, f_j)$ as a function of energy, constitutes the "energy spectrum of the amplitudes of the Fourier-component with frequency f_j", or the "Fourier-resolved spectrum at frequency f_j".

Although some of the objects we study in this work are quite bright (for AGN), it is not possible to study their FR spectra using the full energy resolution offered by *XMM-Newton*. Instead, for each object we extracted light curves in seven bands from 3 to 7 keV with $\Delta E = 0.5$ keV, and also the $7-8$ and $8-10$ keV bands, using a bin size of 100 s. We corrected for the background contribution, estimated the power spectrum (using equation 1), and then subtracted the contribution of the Poisson noise.

In all objects, many of the $P(E_k, f_j)$ values, after the subtraction of the Poisson noise, are negative, especially at the highest energies and frequencies. As a result, the estimation of the respective $R(E_k, f_j)$ is not possible. For this reason, we considered two frequency ranges, namely $10^{-5} - 5\times10^{-4}$ Hz and $5\times10^{-4} - 1\times10^{-3}$ Hz (hereafter the "LF" and "HF" bands). First we estimated the average of the power spectrum estimates in each band, and then we used equation (2) to estimate the average amplitude of the Fourier components in the respective band.

The frequency ranges that we consider are very broad. The LF and HF bands correspond to Fourier components with periods from 10^5 to 2×10^3 s and $2 \times 10^3 - 1000$ s, respectively. This is necessary in order to estimate, as accurately as possible, the average amplitude of the Fourier components, especially in the higher energy bands. However, this choice unavoidably affects the accuracy of the errors of the FR spectra. The error estimation of the average Fourier amplitudes is based on the scatter of the individual amplitudes around their mean in each frequency band. However, due to the red noise character of the AGN power spectra, this scatter is representative, to some degree, of the intrinsic, power-law like dependence of the Fourier amplitudes on frequency. Consequently, the estimated errors of the FR spectra are expected to be overestimated. This effect should depend on the power spectrum slope of each individual source, and is expected to affect more the LF band estimates. In §4 we discuss how we addressed this issue during the FRS model fitting process.

3.1. Interpretation of FRS

The past few years, plots of the energy-dependent variance, σ_E^2, or the rms fractional variability, *i.e.* $r_E = \sigma_E/\langle x_E \rangle$ (where $\langle x_E \rangle$ is the average count rate) as a function of E have become increasingly popular in the study of the spectral variability properties of AGN and GBHs (see for example Edelson et al. 2002, Taylor, Uttley & McHardy 2003, and Markowitz, Edelson & Vaughan 2003 for the application of this method in X–ray variability studies of AGN). Roughly speaking, the variance is equal to the integral of the power spectrum of the source, i.e. $\sigma_E^2 = \int_{1/T}^{\infty} P(E, f) df$, where T is the length of the observed light curve. In practice, this integral can be approximated by the sum: $\sum_j P(E, f_j)\Delta f = \sum_j R^2(E, f_j)$. Consequently, the "rms vs. E" plots and FRS are related analysis methods.

In effect, FRS "decomposes" the rms in each energy band into the contribution of the individual Fourier components. Obviously, the FR spectra provide "more" information, in the same way that a power spectrum provides "more" information than just the variance of a light curve. However, while the variance can be estimated "easily", the requirements for an accurate estimate of the power spectrum are much more demanding. The same is true for FRS and the“rms vs E” plots. We need longer, and high signal-to-noise light curves in order to perform Fourier-resolved spectroscopy, while a rough estimate of the “rms vs E” plot can be achieved with lower quality data.

Although the units of the Fourier-resolved spectra are the same as those of the observed energy spectrum, they *cannot* be interpreted in the same way. While the energy spectrum exhibits the distribution of the emitted flux as a function of energy, the Fourier-resolved spectrum provides the *amplitude of variability* in a certain frequency range, say Δf, as a function of energy. Furthermore, while the integral of the energy spectrum over a certain energy range, say ΔE, is equal to the power emitted from the source over that energy band, the integral of the Fourier-resolved spectrum is equal to the contribution of the Fourier components, in the frequency range Δf, to the variance of the light curve in the energy band ΔE. Consequently, the use of the word “spectrum” for a “$R(E, f)$ vs E” plot can be misleading. We will keep using this term though, as this is what has been used in the past and a change of terminology may cause confusion. However we emphasize again that the Fourier-resolved spectra do *not* show how *photons* are distributed as a function of energy. They simply show how the *variability amplitudes*, at a certain frequency, change with energy.

So, what is the use of these “spectra” in practice? Their important property is that they receive contribution only from the spectral components which are variable on the time scales sampled by the observations. For example, let us consider the case of an AGN with a power-law (PL) X–ray continuum of slope Γ. Suppose now that apart from this PL component, other spectral components (like e.g. reflection from a cold or ionized disk and/or heavy absorption by warm material) also appear in the time-average spectrum of the source. Because of the presence of such components, sometime it is difficult to determine Γ. However, if only the PL component varies in normalization, then, as we show in the Appendix, the Fourier-resolved spectra will have a power-law shape of slope Γ, at all frequencies. Hence, in this case, the FR sectra can not only show the variable component, but provide also an accurate estimation of Γ as well.

A straightforward utility of FRS is found in the study of spectral features that result from reprocessing of the continuum since in this case there exist a natural filter (the light crossing time) which filters out all frequencies higher than $\sim R/c$ (R is the size of the reprocessing area and c the speed of light). Such a feature could be an emission line at energy, say E_0, produced by continuum reprocessing over a region of size R. Should its normalization vary in proportion to the underlying continuum at a given frequency, its EW should remain constant for frequencies $\nu \lesssim R/c$ while it would be vanishing for $\nu \gtrsim R/c$. Lower EW values at a certain frequency range will imply that the line is not “as variable” as the continuum on the respective time scales, either because of the light crossing argument or because the physical condition at the corresponding radius do not favor the presence of the associated transition.

In summary, the Fourier-resolved spectra can show us clearly if and, most importantly, how the various spectral components in the overall energy spectrum of a source vary on the frequency ranges considered. The easiest way to accomplish this, in our case, is to perform a standard model fitting analysis to the FR spectra in the LF and HF bands and then compare the results with those obtained from a similar analysis of the time-average energy spectrum. The model fitting to the time-average spectrum can identify the spectral components which contribute to the emitted radiation from the source. The results from the model fitting of the FR spectra will identify *which* one of the individual spectral components is variable. Any differences between the best fitting parameter values of the time-average spectrum and the LF/HF FR spectra will give us information as to *how* the respective spectral components vary.

We discuss below the results from the application of this method to the data of the five AGN we study in this work.

4. Spectral Analysis & Model Fits

The spectral model fits have been performed with the XSPEC v11.3 package. The errors on the best-fitting model parameters that we report represent the 1σ confidence limit for one interesting parameter. The energy of the emission and absorption features are given in the rest frame of the source. Since the number of points in the mean energy spectrum and the FR spectra is small, whenever possible, we performed the model fitting with the parameters of the emission or absorption features kept fixed at "sensible" values (*i.e.* at 6.4 keV for the iron Kα line and 7.1 keV for the associated absorption edge).

We consider a model as providing an acceptable fit to the data if the null hypothesis probability is larger than 5%. We accept that the addition of a model component is necessary if the quality of the model fitting is improved at more than the 95% significance level. All spectral fits include Galactic absorption, with column values taken from Dickey & Lockman (1990). They are listed on the top of the Tables where we report our best fitting model parameter values.

Spectral responses and the effective area for the pn spectra were generated with the SAS commands *rmfgen* and *arfgen*. Since both the time-average and the FR spectra have a much coarser energy resolution than the intrinsic resolution of the EPIC pn detector, we used the FTOOLS command *rbnrmf* to rebin the original pn response matrix accordingly.

Furthermore, a uniform systematic error of 1% was added quadratically to the statistical error of the time-average spectra to account for all the systematic uncertainties that may be introduced when we undersample the original energy resolution of the instrument and use a "binned" response matrix.

This systematic error was not added to the Fourier-resolved spectra, since as we mentioned above their errors are probably overestimated anyway. In order to resolve this issue we followed a model-dependent procedure. We fitted each FR spectrum with a simple power-law model in the energy bands $3-5.5$ and $7-10$ keV. In most cases, the resulting reduced χ^2 values, χ^2_ν, were significantly smaller than 1. We would then reduce the errors by an appropriate factor (equal to $\sim 2-5$ and $\sim 1.5-4.5$ in the case of the LF and HF spectra, respectively) so that χ^2_ν=1. The resulting error-correction factors were then applied to the $5-7$ keV band points as well.

4.1. Mrk 766

The time-average spectrum and the LF/HF FR spectra of Mrk 766 are plotted in the upper panel of Figure 3 (open circles, filled squares and filled triangles, respectively). The mean spectrum is well fitted by a power law model of $\Gamma_{\rm av} \sim 2.15$ and a broad Gaussian line with $E_{\rm line,av} \sim 6.45$, $\sigma \sim 480$ eV and $\rm EW_{av} \sim 230$ eV. The best fitting model is shown with the dashed line in the upper panel of Figure 3 and the best fitting model parameter values are listed in Table 2. They are in good agreement with the results from the same model fit to the full energy resolution EPIC pn spectrum (see §3.2 in Pounds et al. 2003).

In the lower three panels of the same Figure we plot the Data/Model ratio in terms of "sigmas" (*i.e.*, the error of each point; as a result, the errors of the points in these plots are of size one). In the case of the time-average spectrum, "Model" refers to the best fitting model (with the parameter values listed in Table 2) while in the case of the LF and HF spectra, as "Model" we use the best PL model fit.

The HF spectrum appears to be rather noisy but a PL model ($\Gamma_{\rm HF} \sim 1.9$) fits it rather well. The LF spectrum is also well fitted by a simple PL model ($\Gamma_{\rm LF} \sim 2.2$, χ^2/degrees of freedom (dof)=11.4/8). However, when we add a narrow Gaussian line (*i.e.* σ kept fixed at 100 eV) with $E_{\rm line}$ "frozen" at 6.45 keV (the best fitting value in the case of the time-average energy spectrum) we find that χ^2/dof =5.5/7. According to the F-test, the addition of the narrow line is significant at the 97.1% level.

4.2. NGC 3516

The time-average energy spectrum and the LF FR spectra of NGC 3516 are plotted in the upper panel of Figure 4 (open circles and filled squares, respectively). The $3-10$ keV mean energy spectrum is very flat. This can be explained by the presence of high column layers of absorbing material in various ionization states (Turner et al. 2005). A simple PL model cannot provide an acceptable fit to it. For that reason, we restricted our model fitting to the $4-10$ keV band. We found that a flat PL ($\Gamma_{\rm av} \sim 1.35$; see Table 3) plus a narrow Gaussian line with the centroid energy kept fixed at 6.4 keV (shown with the dashed line on the top panel in Figure 4) can fit the time-average spectrum well.

Since this source shows the smallest amplitude variations, and has the lowest signal-to-noise ratio among the sources in our sample, it is not possible to estimate its HF spectrum. At high frequencies, the intrinsic variations in almost all energy bins are lost in the strong Poisson noise signal. It was possible though to estimate the LF Fourier-spectrum. It is well fitted with a power law model with $\Gamma_{\rm LF} \sim 1.34$. There does appear a small amplitude, positive excess at $E \sim 6.5-7$ keV in the residuals plot, however the addition of a narrow Gaussian line component to the PL model does not improve significantly the goodness of the model fit in this case.

4.3. NGC 3783

NGC 3783 was observed by *XMM-Newton* for two complete orbits between 2001 December 17 and 2001 December 21, producing a total good data exposure of 248 ks. Gaps in the observations due to a telemetry drop-out during the first orbit, and targeting restrictions between the first and second orbits, forced us to analyze the data as three separate observations. Once the Fourier amplitudes of each separate observation segment were calculated, we proceed by combining them in order to calculate the Fourier-resolved spectra for the whole observation.

The energy spectrum of the source above 3 keV is quite complex (Reeves et al. 2004). The time-average spectrum (shown with open circles in the upper panel of Figure 5) is well described by a PL component, together with an iron line at 6.4 keV and an absorption edge at 7.1 keV. Our estimated $\mathrm{EW}_{\rm av}$ of the line (~ 100 eV) is in good agreement with the Reeves et al. (2004) estimate of 107 ± 8 eV (as listed in their Table 1). Our best fitting power law slope though ($\Gamma_{\rm av} \sim 1.5$) is harder than their estimate of ~ 1.7. This is probably caused by the fact that they have considered a combination of a PL plus a cold reflection model (*pexrav* in XSPEC) which naturally results in a steeper PL slope. Due to the reduced energy resolution (i.e. the small number of points in the FR spectra), we cannot really add a reflection component in the modeling of the time-average energy spectrum, as in this case, the best fitting model parameters are essentially unconstrained.

Just like in the case of NGC 3516, despite the availability of long, high signal-to-noise light curves, it was not possible to estimate accurately the HF spectrum of the source. We were able to estimate the LF spectrum though. The lower panel in Figure 5 shows the residuals from the best fitting PL model to the LF spectrum. A PL model does not provide an acceptable fit to the $3-10$ keV LF spectrum ($\chi^2 = 29.9/8$dof). Clearly, a line-like and edge-like feature at ~ 6 keV and ~ 7 keV, respectively, are present in the residuals plot. These features strongly suggest the presence of a variable reflection component, at least on time scales $10^5 - 2 \times 10^3$ sec. Indeed the addition of a narrow Gaussian results in a statistically acceptable fit (the best fitting results are listed in Table 2).

4.4. NGC 4051

We have analyzed two archived XMM observations of NGC 4051. One was taken in 2001, May 16 and the other in 2002, November 22. The source was in a particularly low flux state during the second observation (Uttley et al. 2004; Pounds et al. 2004). The 2001 and 2002 time-average and Fourier-resolved spectra are shown in Figures 6 and 7, respectively. The best fitting results for the 2001 and 2002 spectra are listed in columns 2-4 and 5-6 of Table 5, respectively.

The time-average spectrum during the 2001 observation is well fitted by a $\Gamma_{\rm av} \sim 1.8$ PL model plus a narrow Gaussian line at ~ 6.1 keV ($\mathrm{EW}_{\rm av} \sim 85$ eV) and a 7.1 keV absorption edge ($\tau_{\rm av} \sim 0.1$). Our results are in agreement with those presented in §3.1 and 3.2 of Pounds et al. (2004).

A simple PL model yields a rather poor fit to the 2001 LF spectrum (χ^2 =16.2/8 dof, null hypothesis probability 4%). The respective residuals plot in Figure 6 reveal a positive excess at $6-7$ keV and a deficit at $\sim 7-8$ keV. These features are suggestive for the presence of a reflection component. When we add a narrow Gaussian line, with $\mathrm{E}_{\rm line}$ fixed at the time-average spectrum best fitting value, the fit is now "acceptable", *i.e.*, the null hypothesis probability is now $> 5\%$. On the other hand, the HF spectrum is well fitted by a simple PL model, with $\Gamma_{\rm HF} \sim 2$.

The 2002 time-average spectrum is quite complicated. It is very flat ($\Gamma_{\rm av} \sim 0.9$), a fact that Pounds et al. (2004) explained in terms of partial covering of the central source by ionized material while Uttley et al. (2004) suggested that the reflection component in 2002 is stronger than that during the 2001 observation. A power-law plus a narrow Gaussian line (with a flux of $\sim 1.5 \pm 0.02 \times 10^{-5}$ photon s^{-1} cm^{-2}, in agreement with the Pounds et al. measurement) and a 7.1 keV edge does provide a good fit to the 2002 time-average spectrum.

Due to the short duration of the 2002 observation, the HF Fourier-resolved spectrum could not be determined accurately. The LF spectrum on the other hand is well fitted by a simple PL model. Interestingly, the best-fitting PL slope (~ 1.8) is much steeper than that of the time-average spectrum.

4.5. Ark 564

Ark 564 is an X–ray bright, Narrow Line Seyfert I galaxy, which exhibits large amplitude variations on short time scales. Its time-average spectrum (plotted with open circles in the upper panel of Figure 8) is well fitted by a steep power law ($\Gamma_{\rm av} \sim 2.5$) plus a narrow, weak ($\mathrm{EW_{av}} \sim 85$ eV) Gaussian line at ~ 6.65 keV (see Table 6). These results are in good agreement with those of Papadakis et al. (2007), who have studied the full-resolution pn spectrum of the source.

Its Fourier-resolved spectra are rather simple in shape. They are well fitted by PL models (the best fitting results are listed in Table 6). The FR spectra best fitting slope values are comparable to the best fitting PL slope of the time-average spectrum. The LF residuals' plot is somehow noisy, however, the addition of a narrow Gaussian line at ~ 6.7 keV does not improve significantly the goodness of fit of the PL model.

5. Discussion

We have applied the Fourier frequency-resolved spectral analysis method to *XMM-Newton* data of five AGN with the main aim of studying their spectral variability. This work supplements earlier analysis of the *XMM-Newton* data of MCG 6-30-15 by Papadakis et al. (2005) and work on Galactic sources by a number of other authors (see Introduction). We find that AGN present a much larger variety in the properties of their FR Spectra compared to the (still limited in number) FR spectra of GBHs. We see several obvious reasons for that. First of all, even our longest observation (~ 200 ks) covers a much smaller range, in terms of the objects' characteristic frequency, than the several hours of data of a Galactic source (see discussion in later on in this section). Furthermore, there is evidence that the AGN emission is reprocessed over a larger range of radii than that of Galactic sources, a feature that complicates considerably the comparison between time averaged and FR spectra in AGN. Nevertheless, when we consider the results from the FRS analysis of all the sources together, we can identify some common trends which can be summarized as follows:

1) Both the LF and HF Fourier-resolved spectra of all sources are well fitted by power-law models. We also find that, in general, there are differences between the spectral slopes of the time-average, the LF and the HF spectra. The interpretation of this fact is not apparent at this point; some alternatives are given later on.

2) A line-like feature at energies $\sim 6-6.5$ keV appears the LF spectra of Mrk 766, NGC 4051 and NGC 3873. The most straightforward explanation of these facts is that there is a component of the iron line in these objects that is variable, to some degree, on time scales of the order of a few hours up to a day.

3) We do not detect Fe line features in any of the three HF spectra that we could estimate. This implies the absence of variability of this feature on time scales less than a few hours, despite the significant continuum variations on the same time scales.

5.1. The FRS slope vs frequency relation

The fact that the spectral slopes of the time-average, LF and HF spectra are not always the same implies that the continuum PL in these objects does not vary just in normalization. However, if we consider them individually, it is not easy to interpret the results regarding the slope of the Fourier-resolved spectra ($\Gamma_{\rm FRS}$).

For example, in Mrk 766 and in the 2001 observation of NGC 4051 we observe a $\Delta\Gamma \sim 0.2-0.25$ difference between the slope of the LF and HF spectra ($\Gamma_{\rm LF}$ and $\Gamma_{\rm HF}$, respectively, with the latter being harder). In both cases, the (absolute) difference between the FRS and the time-average spectral slope ($\Gamma_{\rm av}$) is rather small, and of the order of $|\Delta\Gamma| \sim 0.1-0.3$.

The difference $\Gamma_{\rm LF} - \Gamma_{\rm av}$ in the case of NGC 3783 and of the 2002 observation of NGC 4051 is even larger ($\Delta\Gamma \sim 0.5$ and ~ 1, respectively). In both cases, the slope of the LF spectrum ($\Gamma_{\rm LF} \sim 1.8-2$) does make sense, as it is close to the "canonical" slope of the AGN continuum spectrum, suggesting that the intrinsic slope of their X–ray continuum spectrum is indeed $\Gamma \sim 1.8-2$. This result shows clearly the benefits of the Fourier-resolved spectroscopy. The fact then that their time-average spectrum appears to be much flatter must be caused by external factors like absorption by ionized material and/or the substantial contribution from a reflection component.

On the other hand the LF spectrum of NGC 3516 has a slope similar to that of the time-average spectrum of the source (which is harder than the "canonical" value of $\Gamma \sim 1.9-2$).

The same result holds for the LF and HF spectra of Ark 564. They are both as steep as the time-average spectrum of the source.

The picture becomes clearer if we consider all the results together and plot the FR spectral slope as a function of frequency. Since the central source of each AGN in our sample has a different Black Hole (BH) mass, the LF and HF bands correspond to different intrinsic time scales in each system. To this end, we assumed that the LF and HF best PL fitting slope values are representative of the Fourier-resolved spectral slope at the mean frequency of the LF and HF bands (2.55×10^{-4} Hz and 7.5×10^{-4} Hz, respectively). Then, for each object, we divided this frequency with its Keplerian frequency at $3R_S$, $f_{\rm K}(3{\rm R_S})$, where $\rm R_S$ is the Schwarzschild radius. BH mass estimates for NGC 3783, NGC 3516 and NGC 4051 were taken from Peterson et al. (2004). For Ark 564 and Mrk 766, we used the 2.6×10^6 and 3.5×10^6 $\rm M_\odot$ estimates of Botte et al. (2004) and Woo & Urry (2002), respectively.

Figure 9 shows a plot of $\Gamma_{\rm FRS}$ as a function of $f_{\rm norm}$, *i.e.* the frequency normalized as explained above (filled squares, except for Ark 564 and NGC 3783 which are shown separately in the Figure). In the same set of points we have also included the results from the Papadakis et al. (2005) study of MCG-6-30-15. In this case, the mean of the three frequency bands that these authors had considered were normalized to the Keplerian frequency at a distance of $3\rm R_S$ from a BH of mass 4.5×10^6 $\rm M_\odot$ (McHardy et al. 2005). Clearly, taken as a whole, the AGN results suggest that the slopes of the Fourier-resolved spectra harden with increasing frequency. A model of the form $\Gamma_{\rm FRS}\propto \ln f_{\rm norm}^{\alpha}$ describes rather well the AGN data, with $\alpha\sim-0.25$ (solid line in Figure 9).

In the same Figure, we also plot the results of Revnivtsev et al. (1999) and Gilfanov et al. (2000) for Cyg X-1 in its hard/low (LS) and soft/high (HS) state (open squares and open circles, connected with a dashed line, respectively). We have assumed a BH mass of 10 $\rm M_\odot$. The long-dashed line in Figure 9 shows the $\Gamma_{\rm FRS}$ vs $f_{\rm norm}$ best fitting model for the AGN shifted to lower Γ values, appropriate for an extrapolation of the Cyg X-1 data in LS to higher values of $f_{\rm norm}$. At this point, one could consider that, at high frequencies, the $\Gamma_{\rm FRS}$ vs $f_{\rm norm}$ relation is similar both for the AGN we study and Cyg X-1 in its LS, but shifted by $\Delta\Gamma\sim0.5$.

The Ark 564 results (plotted with open diamonds in the same Figure) appear to be consistent with those of Cyg X-1 in its HS. In this state, the $\Gamma_{\rm FRS}$ remains constant up to frequency $\sim0.03f_{\rm K}(3{\rm R_S})$ (*i.e.*, ten times higher than Cyg X-1 in its LS), and then the Fourier-resolved spectra flatten. Consequently, it is our view that the Ark 564 $\Gamma_{\rm FRS}$ are similar to the time-average spectral slope simply because the system operates at a spectral state different than that of the other AGN in our sample and similar to the HS of Cyg X-1. In this latter case, one would have to probe the FR spectra at frequencies higher than those probed to-date in order to observe the decrease of $\Gamma_{\rm FRS}$ with increasing frequency. The NGC 3783 LF slope is also consistent more with the Cyg X-1 data in HS. In fact, the strength of the Fe line in its LF spectrum suggests that this object may indeed be operating like Cyg X-1 in HS (see below).

The dotted line in Figure 9 shows the $\Gamma_{\rm FRS}$ vs $f_{\rm norm}$ best fitting model for the AGN, shifted to higher Γ values, appropriate for the Ark 564 data. One can see that the NGC 3783 Γ_{LF} value consistent with this line, which also seems to be appropriate for an extrapolation of the Cyg X-1 data in HS to higher values of $f_{\rm norm}$.

When we combine together the results from Cyg X-1 and the AGN that we present in this work, the following picture for the accreting black hole systems emerges: a) $\Gamma_{\rm FRS} \sim \Gamma_{av}$, at all frequencies, up to a certain value, say $f_{\rm br}$, b) $f_{\rm br} \sim 0.003 \times f_{\rm K}(3{\rm R_S})$ and $f_{\rm br} \sim 0.03 \times f_{\rm K}(3{\rm R_S})$ for systems in their Low/Hard and High/Soft state, respectively, and c) at frequencies $f > f_{\rm br}$, $\Gamma_{\rm FRS}$ decreases with increasing frequency as $\ln f_{\rm norm}^{-0.25}$, for all systems, irrespective of the state they operate.

We believe that the $\Gamma_{\rm FRS}$-vs.-$f_{\rm norm}$ relation that we present in this work provides new, important clues as to the origin of X–ray spectral variability in AGN. From a phenomenological point of view, our results suggest that the power-law like continuum in AGN does not vary in normalization only. If that were the case, we would expect $\Gamma_{\rm FRS}$ to be constant with $f_{\rm norm}$. We conclude that intrinsic spectral slope variations must occur, although their pattern is not clear at the moment. For example, as we show in the Appendix, $\Gamma_{\rm FRS}$ should not change with $f_{\rm norm}$ even in the case of a pivoting power-law (when the pivot energy is outside the energy range sampled by the observations). Therefore, simple phenomenological models like that of a pivoting energy spectrum can not provide an obvious interpreation of our results.

In general, most models that are available at present do not address the constrains that the Fourier-resolved spectroscopy imposes on the X–ray production mechanism in black hole accreting objects. One exception is Życki (2003) who calculates the FR spectra (and compares them with what is observed in Cyg X-1) in the case when X–ray emission is attributed to active regions moving radially towards the central compact object. In this model, the Comptonized X–ray spectrum from each region is assumed to evolve from softer to harder during the flare evolution as result of diminishing supply of seed photons due to the fact that either the disk is absent at smaller radii or the thickness of the disk's ionized skin increases toward the centre. The model can produce FR spectra whose slope hardens with increasing frequency in a way similar to what we observe in GBHs (and AGN, as we show in this work) assuming the presence of a wide range of infall velocities, and that each such region stimulates the production of other regions as well, in a fashion similar to the "avalanche" model of Poutanen & Fabian (1999) with faster variations appearing later in the spectral evolution of these regions, along with the hardening of their spectra.

However, the predictive power of this model is somehow hampered by the fact that it involves a large number of parameters whose values cannot be predicted in a physical way. For example, one has to assume rather arbitrary if and how the velocity of the regions depends on radius, the maximum/minimum infall velocities, the average value of regions that exist per unit time, the probability that an active region will activate a second one etc. Perhaps the $\Gamma_{\rm FRS}$-vs.-$f_{\rm norm}$ relation that we present in this work can constrain meaningfully the model parameter values and hence help us undertand better their physical implications.

On the other hand, a qualitative account of the FRS results can also be obtained in the simpler case of Advection Dominated Accretion Flows (ADAF; Narayan & Yi 1994), provided that one is willing to accept a relation between the Fourier frequency and the size of the emitting region. In ADAF, for a wide range of accretion rates, the electron temperature attains values typically ~ 100 keV, and remains roughly constant in radius for $x < 10^2 - 10^3$, where x is the radius normalized to $\rm R_S$. Since the local density, $n(x)$, changes with radius as $x^{-3/2}$, the Thompson depth of the flow at radius x, $\tau_T(x)$, should vary as $\tau_T(x) \propto x^{-1/2}$. Consequently, the Comptonization parameter of the flow, $y(x) = \tau_T(x)(kT_e/m_e c^2)$, increases with decreasing radius.

The response of the ADAF to a variation of a particular duration is the convolution of the ACF of the particular variation with the response function of the system. Assuming that the response of the system extends over the entire radial (and hence time) range of the ADAF, a short variation has support mainly in the small values of x, or equivalently the large values of the Comptonization parameter y of the flow. Alternatively, a long duration flare has support over much a larger region of ADAF where the values of y are smaller, the resulting variation is weighted more by the softer photons leading to softer FR spectra. Put it in a different way, short variations produce harder spectra than the long ones.

The above are admittedly qualitative arguments. They are put forward to provide a flavor of the conclusions one can infer from the results of FRS. As such, they seem to provide some support for models which involve hot flows (i.e. ADAF-like geometry) or multiple active regions/perturbations which propagate towards the central object over, say, that of a uniform corona.

5.2. The Iron Line EW vs. Frequency Relation

The lack of response, on short time scales, of the reflection spectrum (including the iron line) on the observed X–ray continuum luminosity variations in AGN has been a long-standing issue (Iwasawa et al. 1996, 1999, Lee et al. 2000, Vaughan & Edelson 2001, Markowitz et al. 2003, Vaughan & Fabian 2004). The present work demonstrates clearly that Fourier-resolved spectroscopy is "sensitive" in detecting iron line variability. Our results suggest that, at least in three out of the five sources in our sample, the iron line is variable on time scales as short as a few hours.

Admittedly, the FRS error-reduction method (see §3) may affect the significance of the line-like features that we detect in the LF spectra of Mrk 766, NGC 3783 and NGC 4051. However, in the case of NGC 3783, the PL best fitting residuals' features around $\sim 5-7$ keV are so strong that, even if we do not reduce the LF errors, the addition of a narrow Gaussian line improves the PL fit at almost the 99% significance level. In Mrk 766, Miller et al. (2006), using a much longer, recent *XMM-Newton* data set have shown that the line flux is indeed variable, in response to the continuum variations, on time-scales of a few ksec. It is only in NGC 4051 that the line detection in its LF spectrum is not highly significant (the addition of a Gaussian line to the PL model is not statistically required; it simply provides a model fit with a null hypothesis probability larger than 5%). Nevertheless, based on the consistency of the NGC 4051's results with those from the other sources (and Cyg X-1) that we present below, we believe that the signal we detect in the LF spectrum of this source is also real.

As with the slope of the FR spectra, it is hard to understand the results regarding the EW of the lines we detect in the three sources if we consider them individually. For example, the EW of the line in the LF spectrum of NGC 3783 (200^{+69}_{-73} eV) is larger than that in the time-average spectrum of the source (100 ± 16 eV). This is strange, as in the simplest case, when both the reflective material and the observer receive the same amount of primary radiation, the maximum value of the line's EW in the FR spectra, in any frequency band, should be no more than the line's EW in the time-average spectrum. This would suggest that the iron line fully responds to the continuum variations, at all frequencies. One could conceivably reconcile these observations by postulating that the average continuum that is determined by the time-average energy spectral studies includes also the contribution from other components not seen by the "cold" matter responsible for its reprocessing to Fe-line photons. In this case, the estimated EW will be smaller than the intrinsic value, which should be at least as large as ~ 200 eV.

In Mrk 766, the EW of the line is smaller in the LF than the time-average spectrum (implying that the line is not "as variable as the continuum", on time scales of ~ 1 hour-1

day) while the situation is less clear in the case of NGC 4051, because of the large uncertainty in the determination of the LF line's EW.

Just like with $\Gamma_{\rm FRS}$, in order to get a deeper insight as to how the iron line varies in AGN, we plot in Figure 10 the EW of the Fe line of the LF FR spectrum, $\rm EW_{FRS}$, for the three objects with positive detection as a function of the Fourier frequency, normalized as explained above. In the same Figure we also plot the results of Revnivtsev et al. (1999) and Gilfanov et al. (200) for Cyg X-1 in LS and HS (open squares and open circles, respectively).

When Cyg X-1 is in its LS, $\rm EW_{FRS}$ remains constant up to frequencies ~ 0.003 of $f_{\rm K}(3\rm R_S)$. At higher frequencies, $\rm EW_{FRS}$ decreases. The dashed line in Figure 10 shows that a model of the form $\rm EW_{FRS} \propto \ln f_{\rm norm}^{-\beta}$ (with $\beta \sim 0.14$) describes rather well the $\rm EW_{FRS}$ vs $f_{\rm norm}$ relation in the case of the Cyg X-1 in LS. Clearly, the NGC 4051 and Mrk 766 results are consistent with the extrapolation of this line to higher frequencies. On the other hand, the surprisingly large $\rm EW_{FRS}$ of NGC 3783 can be explained if the system operates in the same mode as Cyg X-1 in its high state. In this case, $\rm EW_{FRS}$ remains constant at all Fourier-resolved spectra up to ~ 0.05 of $f_{\rm K}(3\rm R_S)$, above which it starts to decrease.

There are however some issues which complicate the analogy between the Cyg X-1 and AGN results. The most puzzling one is the case of Ark 564. The Γ_{HF} and Γ_{LF} values suggest that this source operates in a mode similar to Cyg X-1 in its HS (see discussion in the previous section). If true, we should then expect to detect the iron line in its FR spectrum with a high EW, which is certainly not the case. Recently, Arevalo et al. (2006) suggested that Ark 564 operates like GBHs in their "Very High State". Since the relation between $\rm EW_{FRS}$ and $f_{\rm norm}$ is not known for systems in this state (the results of Reig et al. (2005) suggest that $\rm EW_{FRS}$ in VHS systems is smaller than in HS systems), we cannot make any conclusive statements at the moment.

The $\rm EW_{FRS}$ vs. frequency relation is amenable to a more straightforward interpretation than that of the $\Gamma_{\rm FRS}$ vs. frequency relation, simply because the line emission is the result of reprocessing the X–ray continuum by neutral, or better, sufficiently little ionized, matter. Thus this relation can be used to probe the reprocessing geometry surrounding the X–ray emitting source. The $\rm EW_{FRS}$ dependence on the frequency should be determined mainly by the inverse of the light crossing time between the X–ray source and the reprocessing matter. Gilfanov et al. (2000), assuming the simplified geometry of an isotropic point source at a height of $\sim 10\rm R_S$ above a flat disk, have shown that the decrease of $\rm EW_{FRS}$ at frequencies higher than 0.003 and 0.03 of $f_{\rm K}(3\rm R_S)$, for systems in LS or HS, respectively, can be explained if the distance between the X–ray continuum and the "reflective" part of the disk is ~ 100 and ~ 10 $\rm R_{\it S}$, respectively. Życki (2003, 2004) has also considered the variability properties of the iron Kα line in accreting black holes. He has found that the EW of the line decreases with increasing frequency, in agreement with the results of the Fourier-resolved spectroscopy, even in the case when there is not just one, static source but many, X–ray producing flares/active regions propagating inwards, when the optically thick, cold disk disappeares, gradually, at a distance larger than the radius of the innermost stable orbit, and is replaced by a hot, and less reflective, hot flow.

Interestingly, the normalized frequencies above which $\mathrm{EW_{FRS}}$ decreases with increasing frequency, are very similar to the frequencies above which Γ_{FRS} hardens with increasing frequency. Perhaps then, a combination of a geometrically thin, optically thick disk (which can reflect X–rays) and a hot ADAF, with a transition radius of ~ 100 and $\sim 10-20\mathrm{R_S}$, in the LS and HS systems, can explain, qualitatively, both the Γ_{FRS} and $\mathrm{EW_{FRS}}$ vs frequency relations we observe.

The fact that both $\mathrm{EW_{FRS}}$ and Γ_{FRS} decrease with ν implies a correlation between $\mathrm{EW_{FRS}}$ and Γ_{FRS} as well: at frequencies higher than $0.003-0.03$ of $f_{\mathrm{K}}(3\mathrm{R_S})$, the equivalent width of the line in the FR spectra decreases together with their slope. To the extent that EW can be considered a proxy (for the unobserved) hard X–ray reflection amplitude, R, this relation appears to be similar to the $R-\Gamma$ relation of Zdziarski et al. (1999). Despite the similarities though, one has to take into account that our relation is between "R(ν)" and the slope of the variability amplitudes (at ν) as a function of energy. Our analysis therefore involves the additional timing information not present in the analysis of Zdziarski et al. (1999), who report the relation between quantities determined in the time-average energy spectra.

It is not clear how the $R(\nu)-$ "Γ"(ν) relation that we find relates to the $R-\Gamma$ relation of Zdziarski et al. (1999). These authors accounted for this result in terms of increase in Γ (i.e. softening of the energy spectrum) due to the increase of the number of cooling photons as manifest by the increase of the reflection fraction R (assuming implicitly that the X-ray emission takes place at a geometry fixed for a given source). It is hard to see how one could produce the results we have obtained within this framework.

One possibility was described by Życki (2003) in the context of inwards moving flares whose spectrum evolves (from soft to hard) as they move. The point is that as a result of irradiation by hard X-rays a hot ionized skin forms on the surface of the disk. If the luminosity of the flare increases as it flows inwards, the thickness of the skin increases, the the effectiveness of reprocessing/thermalization decreases: the EW of the line decreases, soft photons diminish, and hence the spectra become harder, at the same time that the variability time scales shorten.

But there are other possibilities as well. As we argued in §5.1, and in Papadakis et al.

(2005), the decrease in Γ with ν maybe due to the variation of the Comptonization parameters with scale (i.e. increasing y with decreasing distance from the central source), as it is the case e.g. in an ADAF. The combination of such a flow attributes with a disk of finite inner radius, implying that the line photons do not respond fully to the high frequency variations of the "harder" spectra, could also then provide a qualitative account of the correlation of the "$\mathrm{R}(\nu)$ vs $\Gamma_{\mathrm{FRS}}(\nu)$" relation.

Testing the above ideas, however, requires a more detailed treatment of the reflection process and the way the reflector responds to the continuum variations. For example, it is important to explain the shape of the $\mathrm{EW}_{\mathrm{FRS}}$ vs frequency relation, but also its "amplitude" as well. The EW of the iron line depends on the ionization state of the reflector (Nayakshin, Kazanas & Kallman 2000), the solid angle subtended by the reflector, and the abundance of iron. The increase of $\mathrm{EW}_{\mathrm{FRS}}$ with decreasing frequency necessarily implies the presence of neutral matter at the corresponding distances intercepting the solid angle implied by the measured $\mathrm{EW}_{\mathrm{FRS}}$. A quantitative investigation of the necessary physical/geometrical arrangement that could explain the observed $\mathrm{EW}_{\mathrm{FRS}}$ values at each frequency requires models far more detailed than warranted by the present investigation; we hope to return to such models in the future.

6. Conclusions

Using long, high signal-to-noise *XMM-Newton* light curves, we estimated the Fourier frequency-resolved spectra of five AGN. The main results from our study are:

1) The slope of the FR spectra in AGN decreases with increasing frequency (as $f^{-0.25}$; see Fig.9) when we take into account properly the differences in the black hole mass of the central engine in these objects. This result shows clearly that the PL continuum in AGN must vary in slope, as well as in normalization, with time.

2) We detect significant evidence in the LF spectrum of three objects (Mrk 766, NGC 3783, and NGC 4051) that the iron line is responding to the continuum variations, on time scales larger than a few hours.

3) We do not detect any evidence of Fe line features in our HF spectra. This result indicates that the iron line does not respond to the significant continuum variations on time scales less than an hour.

We note that, apart from providing answers to questions like "is the Fe line variable?", Fourier frequency-resolved spectroscopy can show *how* the line emission responds to the continuum variations at certain time scales. The data so far suggest that the relation between $EW_{\rm FRS}$ and $f_{\rm norm}$ (*i.e.* $EW_{\rm FRS}$ decreasing with increasing $f_{\rm norm}$) is similar in AGN and Cyg X-1.

The interpretation of these results is not straightforward. The accounts we have presented in §5.1 and 5.2 may or may not be correct. Their importance lies in indicating the potential of the FRS method in probing the accretion flow structure of AGN and GBHs. We are encouraged, for instance, by the way that the NGC 3783 and the 2002 NGC 4051 observation FRS results can be consolidated within a reasonable, coherent scheme, whereby the intrinsic primary PL slope is $\sim 1.8 - 2$, hence the flatness of the time-average spectrum is caused by external effects.

We believe that both the continuation of a systematic study with this method, but also the effort to develop theoretical models that can describe, quantitatively, the data as well, have a great potential for providing a more complete and consistent picture of these objects. Significant progress in the determination of the $\Gamma_{\rm FRS}$ and $\rm EW_{FRS}$ vs $f_{\rm norm}$ relation in AGN, and its comparison with the respective relations in GBHs, can be made with the use of light curves which will allow us to study variations which operate on time scales longer than a few days. In retrospect, if we look at Figures 9 and 10, it seems rather surprising that we could estimate $\Gamma_{\rm FRS}$, or detect line-like features, in any for the AGN Fourier-resolved spectra that we studied in this work. The reason is that when compared to Cyg X-1, after taking into account the difference in the BH mass of the systems, the frequencies we probe in AGN with the present *XMM-Newton* light curves are significantly higher than those that have been studied in GBHs with *RXTE* data. To this end, the numerous, high signal-to-noise, long monitoring light curves in the *RXTE* archive will be helpful. Their analysis with the FRS method will allow us to determine accurately the $\Gamma_{\rm FRS}$ and $\rm EW_{FRS}$ relations in AGN. We plan to perform such a research work in the near future.

IEP and ZI gratefully acknowledge support for this work by the General Sectreteriat of Research and Technology of Greece. DK acknowledges support by a *Chandra* GO grant.

A. Appendix: Calculation of the FR spectra in some simple cases

According to equation (2) in §3, the Fourier resolved spectrum, $R(E,f)$, of a stationary process is defined as $\sqrt{P(E,f)df}$ (where $P(E,f)$ is the power spectral density function of the process). Suppose now that the X–ray energy spectrum, $F(E,t)$, of an AGN is given by

$$F(E,t) = A(E)[B(E,t) + C(E)],$$

where $B(E,t)$ represents the continuum, time variable emission of the source, $C(E)$ represents any spectral components that may be present and do not vary with time (i.e. X–ray reflection from distant material) and $A(E)$ stands for spectral components that modify the continuum emission (like cold and/or warm absorption, absorption edges etc).

In order to calculate the FRS we need first to estimate the PSD of $F(E,t)$. For a real valued, stationary process we have,

$$P(E,f) = \int_{-\infty}^{+\infty} \cos(2\pi f\tau) ACF(E,\tau) d\tau,$$

where

$$ACF(E,\tau) =$$

$$\langle [F(E,t) - \langle F(E,t)\rangle][F(E,t+\tau) - \langle F(E,t)\rangle]\rangle$$

is the autocovariance function of $F(E,t)$ at lag τ.

For example, let us consider the simple case of power-law like continuum, where only the normalization (at 1 keV) varies with time, i.e. $B(E,t) = K(t)E^{-\alpha}$. In this case,

$$\langle F(E,t)\rangle = A(E)[\langle K(t)\rangle E^{-\alpha} + C(E)]\ .$$

It is easy to show that

$$ACF(E,\tau) = A^2(E)E^{-2\alpha} ACF_K(\tau),$$

where $ACF_K(\tau)$ is the autocovariance function of $K(t)$. Consequently,

$$P(E,f) = A^2(E)E^{-2\alpha} P_K(f),$$

and hence

$$R(E,f) = A(E)E^{-\alpha}\sqrt{P_K(f)df}.$$

In other words, in the case when the X–ray energy spectrum of an AGN has a power-law like shape with a slope of α and varies only in normalization, then the FR spectra also have a power-law shape, with slope equal to α, at *all* frequencies. Any constant components that may be present in the time-average spectrum, and may complicate the correct determination of the continuum slope, will not appear in the FR spectra. In this case, it may be easier to determine the intrinsic spectral slope from the model fitting of the FR spectra rather than of the time-average spectrum.

We note that if $A(E) = \exp[-n_{\rm H}\sigma(E)]$, i.e. the spectrum is absorbed by an external absorber with constant column density, or $A(E) = \exp[-D(E/E_c)^{-3}]$ where E_c is the threshold energy of an absorption edge (with constant absorption depth D), then the FRS will also show the signs of the absorption effects at the same energies, and with the same strength, as in the time-average spectrum of the source.

Suppose now that $C(E)$ is also variable with time. For example, let us assume that there is an emission line in the spectrum (at E_L) whose flux varies with time, i.e.

$$C(E,t) = \frac{L(t)}{\sqrt{\sigma(2\pi)}} e^{-(E-E_L)^2/2\sigma^2}.$$

In this case,

$$\langle F(E,t) \rangle =$$
$$A(E) \left\{ \langle K(t) \rangle E^{-\alpha} + \frac{\langle L(t) \rangle}{\sqrt{\sigma(2\pi)}} e^{-(E-E_L)^2/2\sigma^2} \right\}$$

where σ is the width of the line. In the simple case when the line is produced by isotropic irradiation of matter in the innermost part of an accretion disk by the X–ray continuum source, one would expect the bulk of the line to respond in synchrony with the continuum variations and hence $L(t) \sim cK(t)$ (where c is a constant). One can show that in this case

$$ACF(E,\tau) = A(E)^2 \times$$
$$\times \left\{ (E)^{-\alpha} + \frac{c}{\sqrt{\sigma(2\pi)}} e^{-(E-E_L)^2/2\sigma^2} \right\}^2 ACF_K$$

and hence

$$P(E,f) = A(E)^2 \times$$
$$\left\{ (E)^{-\alpha} + \frac{c}{\sqrt{\sigma(2\pi)}} e^{-(E-E_L)^2/2\sigma^2} \right\}^2 P_K(f).$$

Consequently, the FRS will be given by

$$R(E,f) = A(E) \times$$
$$\times \left\{ E^{-\alpha} + \frac{c}{\sqrt{\sigma(2\pi)}} e^{-(E-E_L)^2/\sigma^2} \right\} \sqrt{P_K(f)df}\ .$$

The amplitude of the line relative to the continuum (i.e. the line's EW) will be the same in both the time averge and the FR spectra of all frequencies.

Finally let us consider the case of a power law with a variable slope, i.e. the case when $B(E,t) = K(E/E_P)^{-\alpha(t)}$ (where E_P is the pivot energy). If σ_α^2 is significantly smaller than

α (a condition that probably holds in the case of many AGN where typically $\alpha \sim 1$ and $\sigma_\alpha^2 \sim 0.1$), then it can be shown that

$$ACF(E,\tau) = A(E)^2 \times$$

$$\times K^2 (E/E_P)^{-2\langle\alpha\rangle} \ln^2(E/E_C) ACF_\alpha(\tau).$$

Subsequently,

$$P(E,f) = A(E)^2 K^2 (E/E_P)^{-2\langle\alpha\rangle} \ln^2(E/E_P) P_\alpha(f),$$

and the FR spectra will be given by the relation,

$$R(E,f) = A(E) K \left(\frac{E}{E_P}\right)^{-\langle\alpha\rangle} \ln\left(\frac{E}{E_P}\right) \sqrt{P_\alpha(f) df}.$$

If E_P is located within the energy range ($E_{\min} - E_{\max}$) at which the FR spectra are estimated, the Fourier-resolved spectra will *not* have a power-law shape. Instead, significant curvature will appear around E_P. If on the other hand E_P is outside the energy range that is considered, the deviation of the Fourier-resolved spectra from a power law shape with slope equal to the time-average α ($\langle\alpha\rangle$) may not be noticed. Hence, even in the case of a pivoting energy spectrum, we expect the FRS to have the *same* slope ($\sim \langle\alpha\rangle$) at all frequencies.

REFERENCES

Arevalo, P., Papadakis, I.E., Uttley, P., McHardy, I.M., & Brinkmann, W. 2006, MNRAS, 372, 401

Botte, V., Ciroi, S., Rafanelli, P., & Di Mille, F. 2004, AJ, 127, 3168

Dickey, J.M., & Lockman, F.J. 1990, ARA&A, 28, 215

Edelson, R., Turner, T.J., Pounds, K., Vaughan, S., Markowitz, A., Marshall, H., Dobbie, P., & Warwick, R. 2002, ApJ, 568, 610

Gilfanov, M., Revnivtsev, M., & Molkov, S. 2003, A&A, 410, 217

Gilfanov, M., & Revnivtsev, M. 2005, AN, 326, 812

Iwasawa, K., et al., 1996, MNRAS, 282, 1038

Iwasawa, K., Fabian, A.C., Young, A.J., Inoue, H. & Matsumoto, C. 1999, MNRAS, 306, L19

Kazanas, D., Hua, X.-M., & Titarchuk, L. 1997, ApJ, 480, 735

Lee, J.C., Fabian, A.C., Reynolds, C.S., Brandt, W.N. & Iwasawa, K. 2000, MNRAS, 318, 857

Markowitz, A., Edelson, R. & Vaughan, S. 2004, ApJ, 598, 935

Miller, L., Turner, T.J., Reeves, J.N., George, I.M., Porquet, D., Nandra, K., & Dovciak, M. 2006, A& A, 453, L13

M^{c}Hardy, I.M., Gunn, K.F., Uttley, P., & Goad, M. R. 2005, MNRAS, 359, 1469

Nandra, K., George, I. M., Mushotzky, R. F., Turner, T. J., & Yaqoob, T. 1997, ApJ, 477, 602

Narayan, R., & Yi, I. 1994, ApJ, 428, L13

Nayakshin, S., Kazanas, D., & Kallman, T. R. 2000, ApJ, 537, 833

Papadakis, I.E., Brinkmann, W., Page, M.J., M^{c}Hardy, I., & Uttley, U. 2007, A&A, 461, 931

Papadakis, I.E., Kazanas, Demosthenes, & Akylas, A. 2005, ApJ, 2005, 631, 727

Peterson, B. M., et al. 2004, ApJ, 613, 682

Pounds, K.A., Reeves, J.N., Page, K.L.; Wynn, G.A., & O'Brien, P.T. 2003, 342, 1147

Pounds, K.A., Reeves, J.N., King, A.R., & Page, K.L. 2004, MNRAS, 350, 10

Poutanen, J., & Fabian, A. C. 1999, MNRAS, 306, L31

Priestley, M.B. 1989, Spectral Analysis and Time Series (London, Academic Press Limited)

Reeves, J.N., Nandra, K., George, I.M., Pounds, K.A., Turner, T.J., & Yaqoob, T. 2004, ApJ, 602, 648

Reig, P., Papadakis, I.E., Shrader, C.R., & Kazanas, D. 2006, ApJ, 644, 424

Revnivtsev, M., Gilfanov, M., & Churazov, E. 1999, A&A, 347, 23

Revnivtsev, M., Gilfanov, M., & Churazov, E. 2000, MNRAS, 316, 923

Revnivtsev, M., Gilfanov, M., & Churazov, E. 2001, A&A, 380, 520

Sobolewska, M.A., & Życki, P.T. 2006, MNRAS, 370, 405

Taylor, R.D., Uttley, P., & M^{c}Hardy, I. M. 2003, MNRAS, 342, L31

Turner, T.J., Kraemer, S.B., George, I.M., Reeves, J.N., & Bottorff, M.C. 2005, ApJ, 618, 155

Uttley, P., Taylor, R.D., M^{c}Hardy, I.M., Page, M.J., Mason, K.O., Lamer, G., & Fruscione, A. 2004, 347, 1345

Vaughan, S. & Edelson, R. 2001, ApJ, 548, 694

Vaughan, S. & Fabian, A.C. 2004, MNRAS, 348, 1415

Woo, J-H, & Urry, C.M. 2002, ApJ, 579, 530

Zdziarski, A. A., Lubinski, Piotr & Smith, D. A. 1999, MNRAS, 303, L11

Życki, P. 2003, MNRAS, 340, 639

Życki P. 2004, MNRAS, 351, 1180

This preprint was prepared with the AAS LaTeX macros v5.2.

Table 1. Details of the observations used in the present work.

Name	Date	Exp. Time	Obs ID	PI	Filter	Mode
Mrk 766	2001/05/20	100 ks	0109141301	Mason	Medium	Small Window
NGC 3516	2001/04/10	88 ks	0107460601	Mushotzky	Thin	Small Window
NGC 3783	2001/12/17	125 ks	0112210201	Kaastra	Medium	Small Window
	2001/12/19	123 ks	0112210501	Kaastra	Medium	Small Window
NGC 4051	2001/05/16	101 ks	0109141401	Mason	Medium	Small Window
	2002/11/22	34 ks	0157560101	Jansen	Medium	Large Window
Ark 564	2005/01/05	100 ks	0206400101	Papadakis	Medium	Small Window

Table 2. The Mrk 766 best model fitting results ($N_H = 1.7 \times 10^{20} cm^{-2}$)

Parameter	Mean	LF	HF
Γ	2.14 ± 0.02	2.19 ± 0.04	1.93 ± 0.11
E_{line} (keV)	6.45 ± 0.10	6.45[a]	–
σ_{line} (eV)	480 ± 100	100[a]	–
EW (eV)	230^{+20}_{-50}	60^{+70}_{-35}	–
χ^2/d.o.f.	6.2/5	5.5/7	12.2/7

[a]Parameter kept fixed

Table 3. The NGC 3516 best model fitting results ($N_H = 2.9 \times 10^{20} cm^{-2}$)

Parameter	Mean	LF
Γ (keV)	1.34 ± 0.03	1.34 ± 0.11
E_{line} (keV)	6.4[a]	–
σ_{line} (eV)	100[a]	–
EW (eV)	130 ± 0.15	–
χ^2/d.o.f.	7.7/4	10.6/8

[a]Parameter kept fixed

Table 4. The NGC 3783 best model fitting results ($N_H = 8.3 \times 10^{20} cm^{-2}$)

Parameter	Mean	LF
Γ	1.46 ± 0.01	1.94 ± 0.02
E_{line} (keV)	6.4^a	6.05 ± 0.31
σ_{line} (eV)	100^a	100^a
EW (eV)	100 ± 16	200^{+69}_{-73}
E_{edge} (keV)	7.1^a	–
τ_{edge}	0.12 ± 0.07	–
χ^2/d.o.f.	5.3/6	7.8/6

[a]Parameter kept fixed

Table 5. The 2001 and 2002 NGC 4051 best model fitting results ($N_H = 1.3 \times 10^{20} cm^{-2}$)

Parameter	Mean(01)	LF(01)	HF(01)	Mean(02)	LF(02)
Γ	1.79 ± 0.02	2.17 ± 0.04	1.99 ± 0.19	0.88 ± 0.03	1.83 ± 0.17
E_{line} (keV)	6.10 ± 0.20	6.10[a]	–	6.4[a]	–
σ_{line} (eV)	100[a]	100[a]	–	100[a]	–
EW (eV)	84 ± 12	41^{+38}_{-35}	–	191 ± 20	–
E_{edge} (keV)	7.1[a]	–	–	7.5 ± 0.1	–
τ_{edge}	0.11 ± 0.03	–	–	0.75 ± 0.12	–
χ^2/d.o.f.	5.1/5	12.8/7	7.9/8	9.8/5	6.5/10

[a]Parameter kept fixed

Table 6. The Ark 564 best model fitting results ($N_H = 6.4 \times 10^{20} cm^{-2}$)

Parameter	Mean	LF	HF
Γ	2.45 ± 0.02	2.51 ± 0.05	2.53 ± 0.46
E_{line} (keV)	6.65 ± 0.20	–	–
σ_{line} (eV)	100[a]	–	–
EW (eV)	84^{+19}_{-17}	–	–
χ^2/d.o.f.	3.8/6	9.6/8	6.1/7

[a]Parameter kept fixed

Fig. 1.— The full band, 0.2 – 10 keV, light curves of Mrk 766, NGC 3516, and NGC 3783 in bins of size 100 s. The light curves are normalized to the lowest count rate, in order to reveal clearly the observed variability amplitude in each case.

Fig. 2.— Same as with Figure 1 in the case of the NGC 4051 and Ark 564 full band light curves.

Fig. 3.— Upper panel: The time-average (*i.e.*, "mean"), LF and HF Fourier-resolved spectra of Mrk 766 (open circles, filled squares and triangles, respectively). The dashed lines show the best fitting model in the case of the time-average spectrum, and the best fitting simple Power-Law model in the case of the LF and HF spectra. Lower panels: Plot of the best model fitting residuals in the case of the time-average spectrum, and of the best PL model fitting residuals in the case of the LF and HF spectra.

Fig. 4.— Same as with Figure 3 in the case of the time-average and the LF spectrum of NGC 3516.

Fig. 5.— Same as with Figure 3 in the case of the time-average and the LF spectrum of NGC 3783.

Fig. 6.— Same as with Figure 3 in the case of the time-average, the LF and HF spectrum of NGC 4051 (May 2001 observation).

Fig. 7.— Same as with Figure 3 in the case of the time-average and the LF spectrum of NGC 4051 (November 2002 observation).

Fig. 8.— Same as with Figure 3 in the case of the time-average , the LF and HF spectrum of Ark 564.

Fig. 9.— The Fourier-resolved spectral slope of AGN, including the results of Papadakis et al. (2005) on MCG -6-30-15, plotted as a function of the Fourier frequency normalized to the Keplerian frequency at $3R_S$ (filled squares). The Ark 564 and NGC 3873 results are plotted with different symbols for the reasons discussed in the text. The open squares and circles show the Cyg X-1 results in the case when the system is at its Low and High state, respectively. The solid line shows the best fitting model to the AGN data. The long dashed and dotted lines have the same slope but are shifted to lower and higher Γ_{FRS} values, respectively, in order to match the Cyg X-1 results in LS and HS.

Fig. 10.— The EW of the iron-line which is detected in the LF spectra of NGC 4051, Mrk 766, and NGC 3783 plotted as a function of the Fourier frequency normalized to the Keplerian frequency at $3R_S$ (filled squares; the sequence as given above from left to right).

Open squares and circles show the Cyg X-1 results in the case when the system is at its Low and High states, respectively. The dashed line shows the best fitting model to the Cyg X-1 at frequencies above ~ 0.005 of $f_{\rm K}(3{\rm R_S})$.

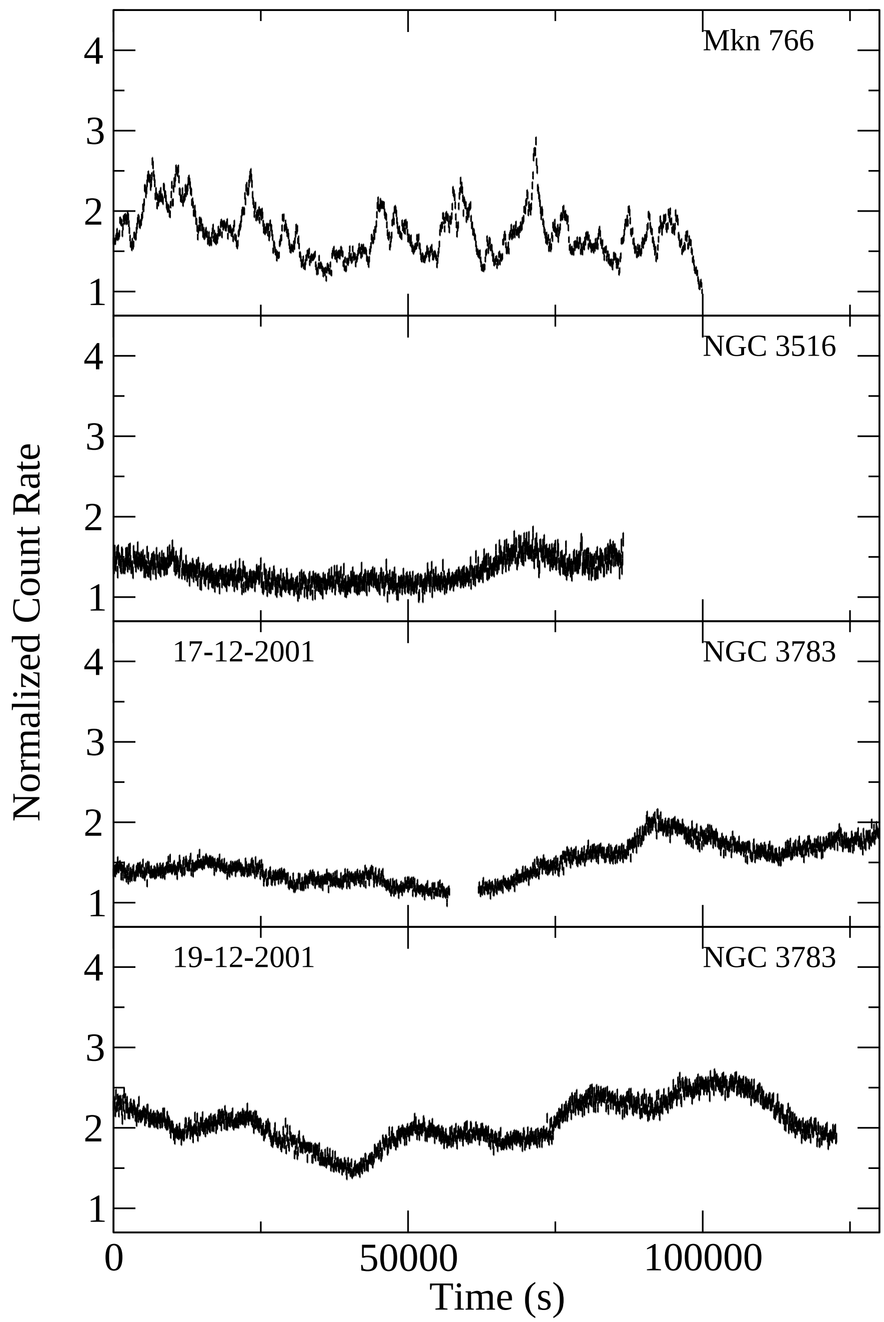
Mkn 766
NGC 3516
17-12-2001
NGC 3783
19-12-2001
NGC 3783
Normalized Count Rate
1
2
3
4
0
50000
100000
Time (s)

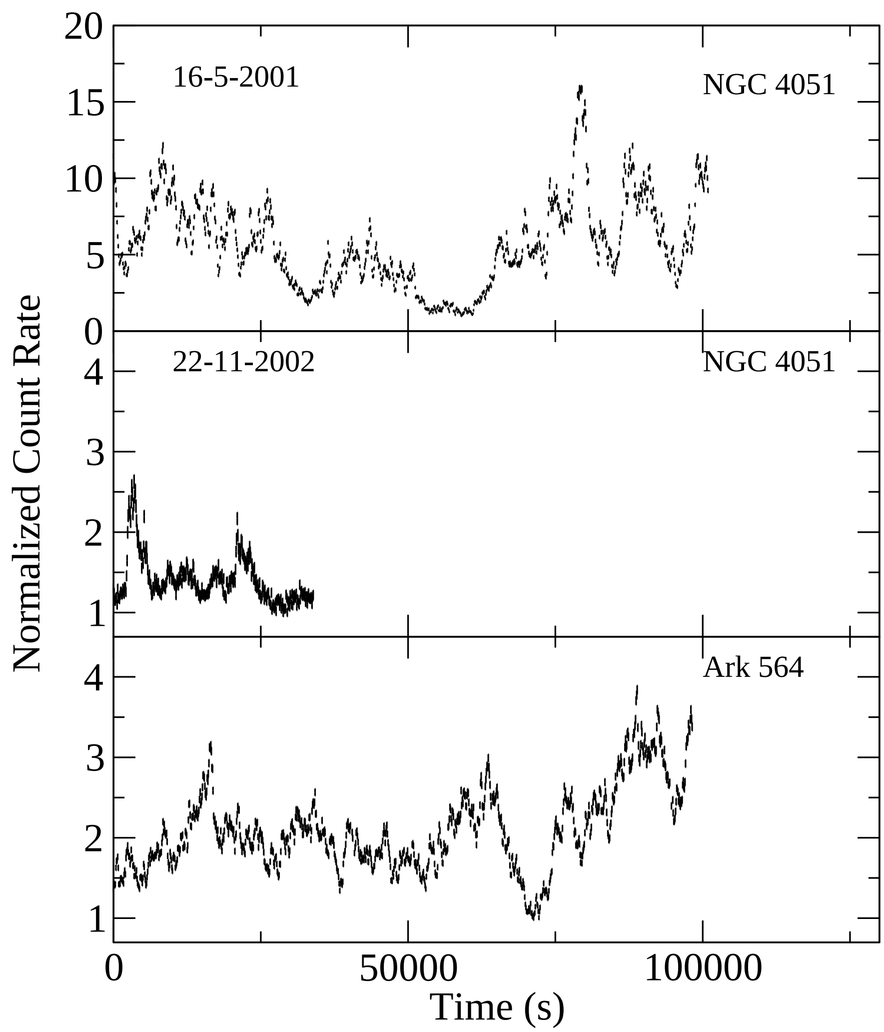
16-5-2001
NGC 4051
22-11-2002
NGC 4051
Ark 564
Normalized Count Rate
Time (s)
0
5
10
15
20
1
2
3
4
1
2
3
4
0
50000
100000

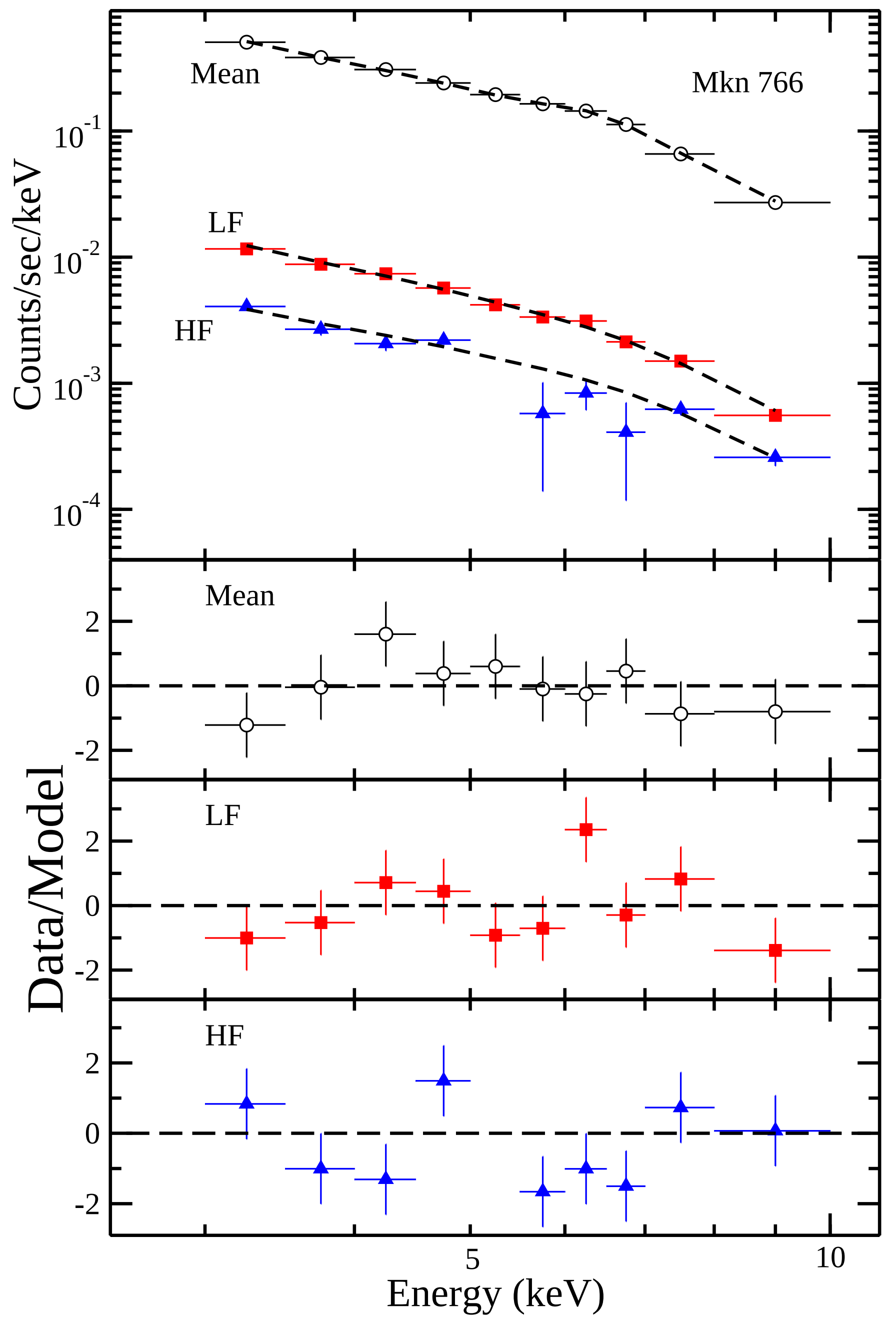

Mean
Mkn 766
LF
HF
Counts/sec/keV
10^{-1}
10^{-2}
10^{-3}
10^{-4}
Data/Model
Mean
LF
HF
2
0
-2
5
10
Energy (keV)

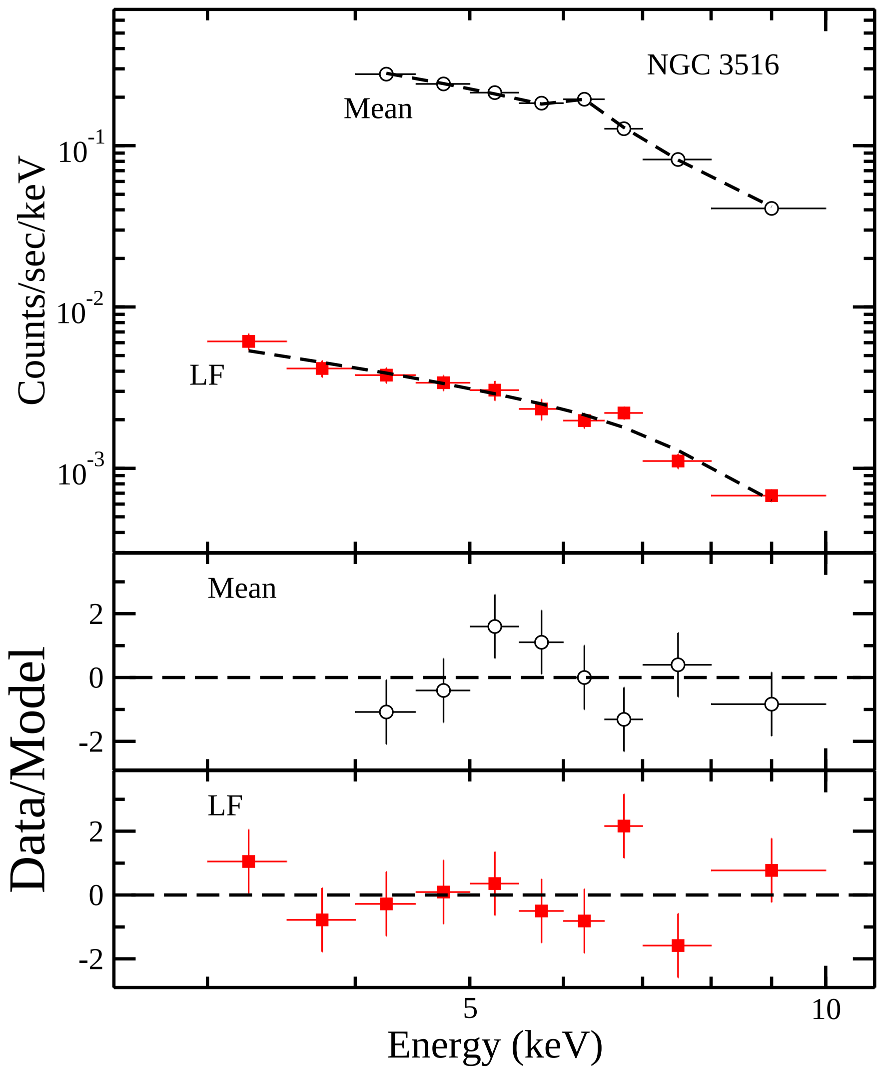
NGC 3516
Mean
LF
Counts/sec/keV
10^{-1}
10^{-2}
10^{-3}
Mean
LF
Data/Model
2
0
-2
5
10
Energy (keV)

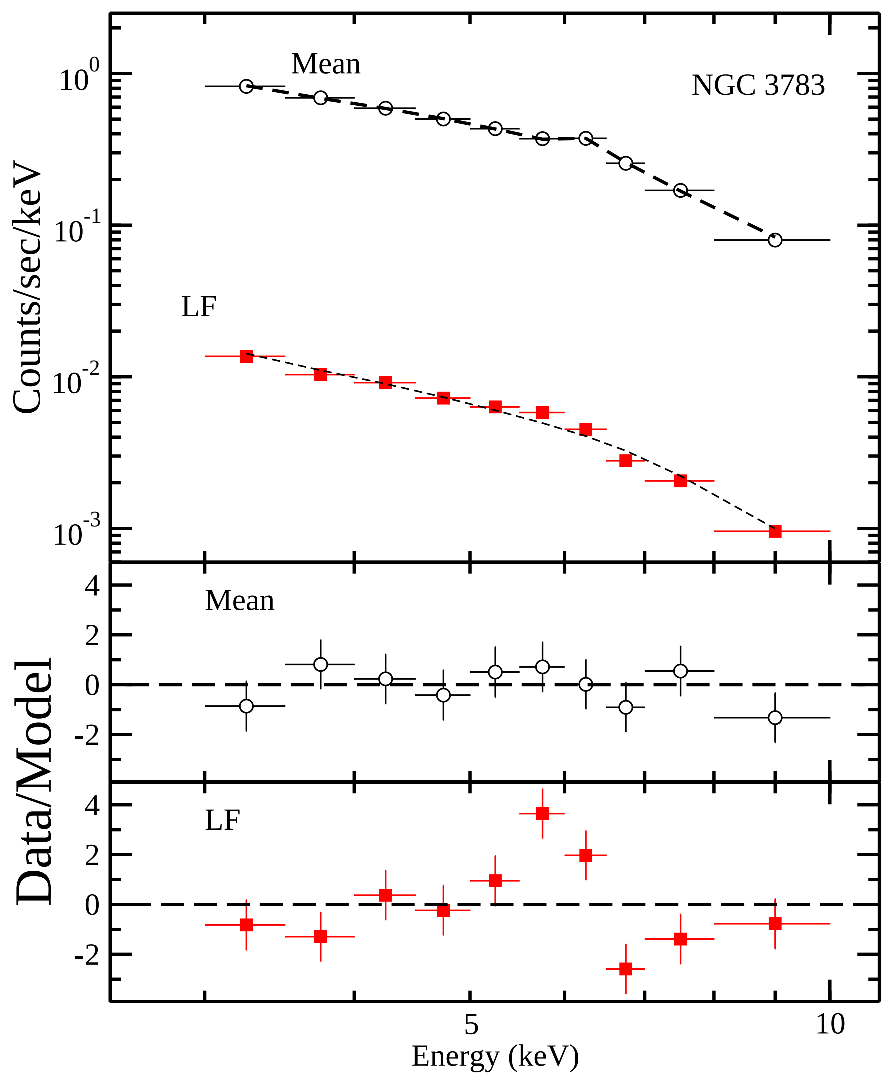
Mean
NGC 3783
LF
Counts/sec/keV
10^0
10^{-1}
10^{-2}
10^{-3}
Mean
LF
Data/Model
4
2
0
-2
5
10
Energy (keV)

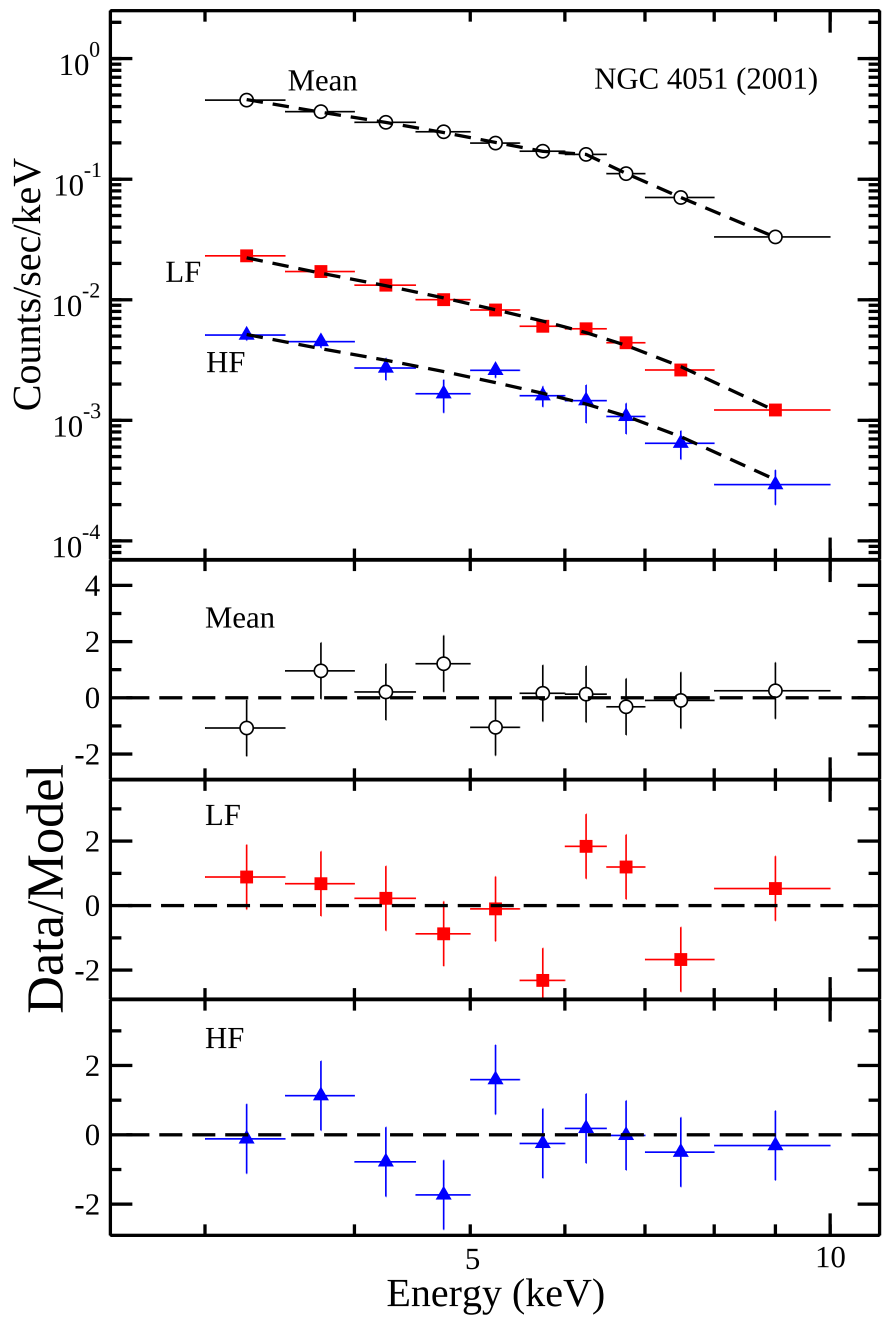

NGC 4051 (2001)
Mean
LF
HF
Counts/sec/keV
Data/Model
Energy (keV)

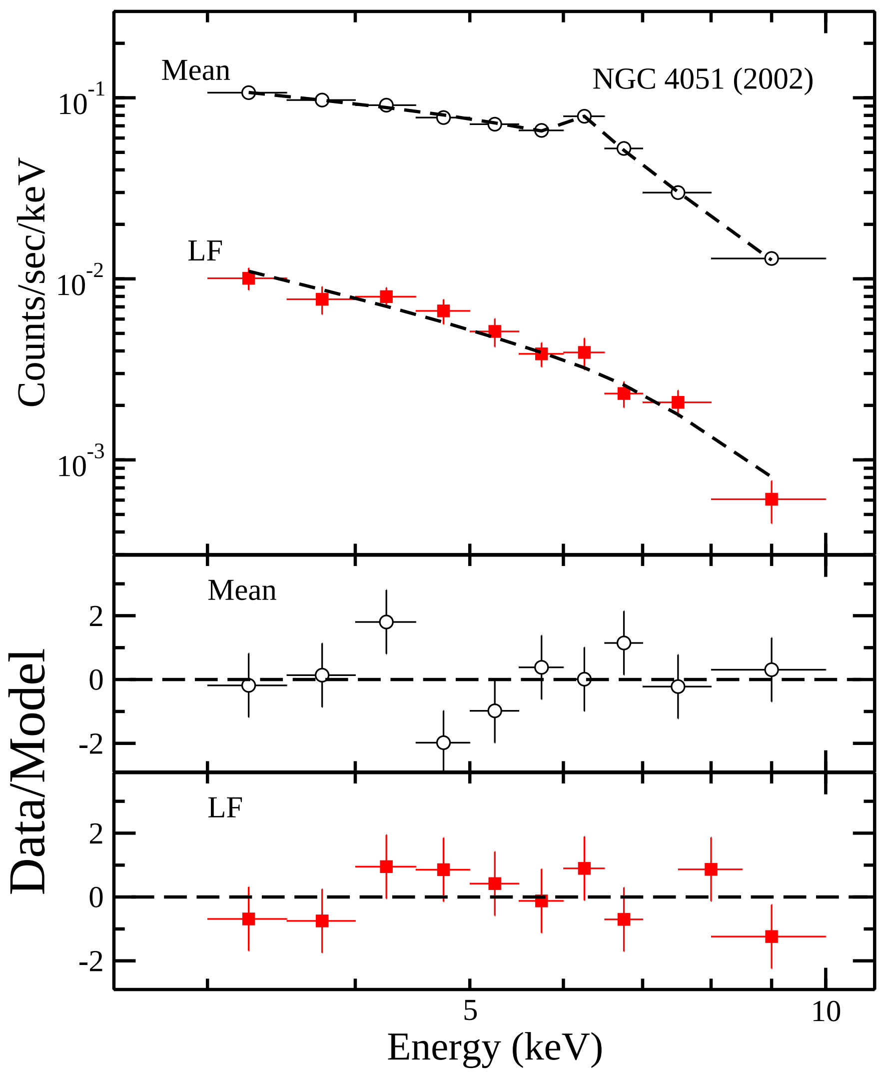
Mean
NGC 4051 (2002)
LF
Counts/sec/keV
Data/Model
Mean
LF
Energy (keV)

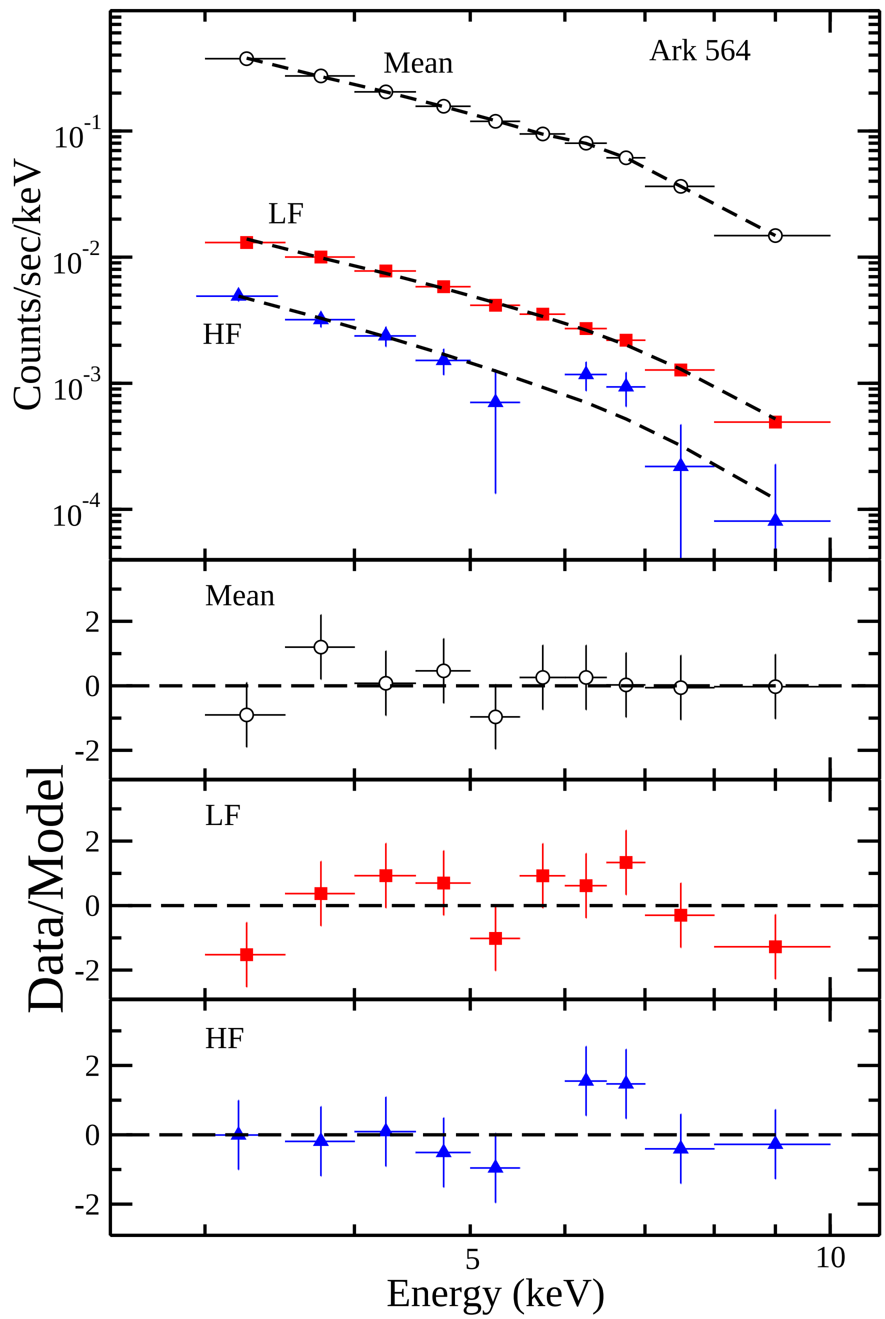

Ark 564
Mean
LF
HF
Counts/sec/keV
10^{-1}
10^{-2}
10^{-3}
10^{-4}
Mean
LF
HF
Data/Model
2
0
-2
5
10
Energy (keV)

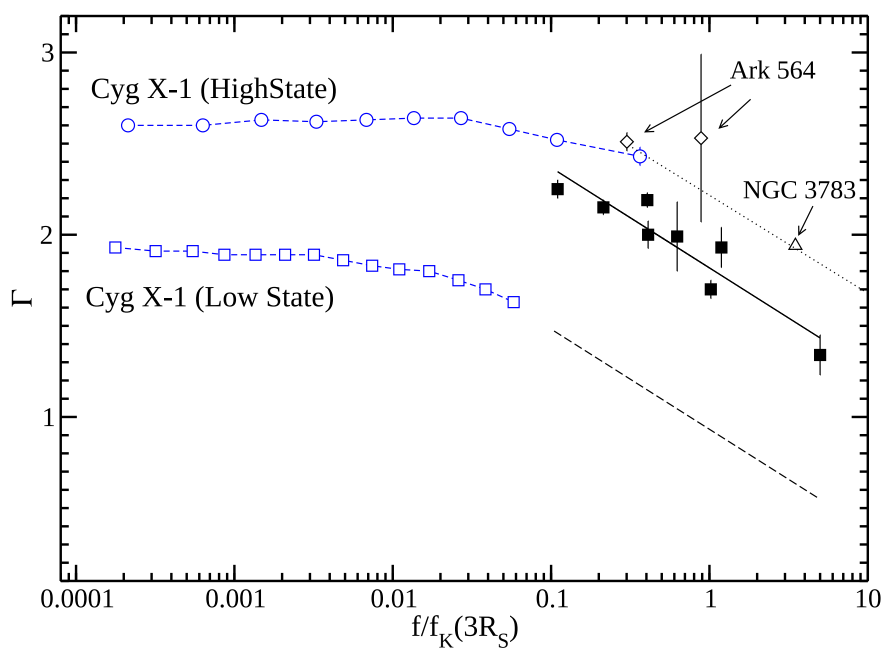
Cyg X-1 (HighState)
Cyg X-1 (Low State)
Ark 564
NGC 3783
Γ
3
2
1
0.0001
0.001
0.01
0.1
1
10
$f/f_K(3R_S)$

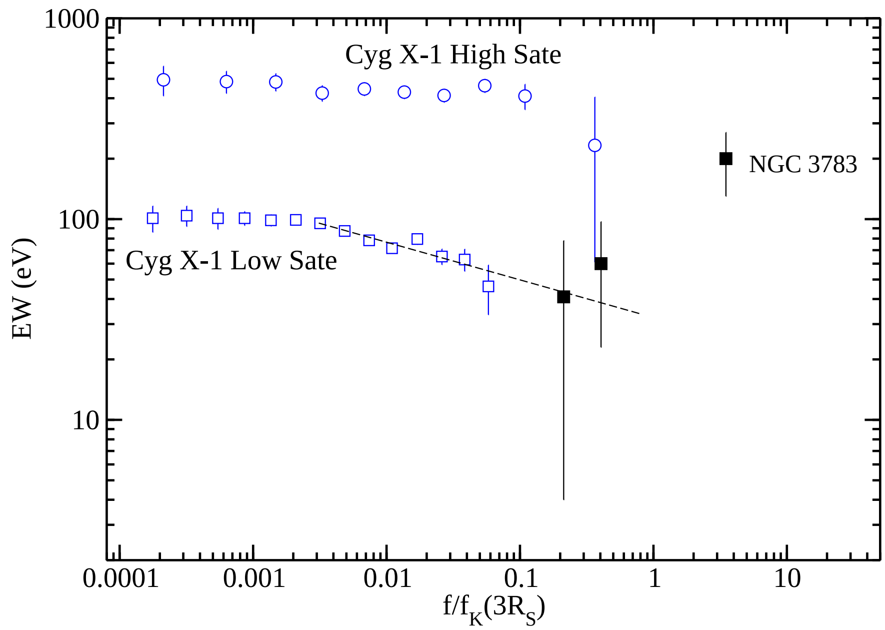
Cyg X-1 High Sate
NGC 3783
Cyg X-1 Low Sate
1000
100
10
EW (eV)
0.0001
0.001
0.01
0.1
1
10
$f/f_K(3R_S)$